Mon. Not. R. Astron. Soc. **396,** 1038–1045 (2009) doi:10.1111/j.1365-2966.2009.14770.x

Studies of accretion flows around rotating black holes – III. Shock oscillations and an estimation of the spin parameter from QPO frequencies

S. Mondal,[1,2] P. Basu[2⋆] and S. K. Chakrabarti[3,2]†

[1]*R. K. Mission Residential College, Narendrapur, Kolkata, India*
[2]*Indian Centre for Space Physics, Garia, Kolkata, India*
[3]*S.N. Bose National Centre for Basic Sciences, Salt Lake, Kolkata, India*

Accepted 2009 March 11. Received 2009 March 9; in original form 2009 January 8

ABSTRACT

In the present communication of our series of papers dealing with the accretion flows in the pseudo-Kerr geometry, we discuss the effects of viscosity on the accretion flow around a rotating black hole. We find the solution topologies and give special attention to the solutions containing shocks. We draw the parameter space where standing shocks are possible and where the shocks could be oscillating and could produce quasi-periodic oscillations (QPOs) of X-rays observed from black hole candidates. In this model, the extreme locations of the shocks give the upper limits of the QPO frequencies ($\nu_{\rm QPO}$) which could be observed. We show that both the viscosity of the flow and the spin of the black hole a increase the QPO frequency while, as expected, the black hole mass reduces the QPO frequencies. Our major conclusion is that the highest observed frequency gives a strict lower limit of the spin. For instance, a black hole exhibiting $\nu_{\rm QPO} \sim 400$ and 700 Hz must have the spin parameters of $a > 0.25$ and >0.75, respectively, provided viscosity of the flow is small. We discuss the implications of our results in the light of observations of QPOs from black hole candidates.

Key words: instabilities – accretion, accretion discs – black hole physics – hydrodynamics – Shock waves.

1 INTRODUCTION

In the standard theory of thin accretion flows around black holes (Shakura & Sunyaev 1973, hereafter SS73) viscosity plays a major role. Viscosity transports angular momentum outwards and allows matter to sink into the potential well formed by the central compact object. In this model, the flow angular momentum is assumed to be Keplerian and this is the standard notion about how matter is accreted. However, Chakrabarti & Molteni (1995) and Lanzafame, Molteni & Chakrabarti (1998), through extensive numerical simulations, showed that the angular momentum distribution depends on the viscosity parameter. They showed that close to a black hole, the disc does not have a Keplerian distribution. This is because the flow must be supersonic on the horizon (Chakrabarti 1990) whereas a Keplerian disc is always subsonic (SS73). A study based on observed data from XTE J1550−564 also suggests the existence of the sub-Keplerian flow (Wu & Soria 2002). Smith et al. (2001) and Smith, Heindl & Swank (2002) also mentioned that effects of changes in time-scales shorter than the viscous time have been observed in several black hole candidates, leading them to believe that sub-Keplerian flows are certainly playing a role. Since a sub-Keplerian flow can also produce standing and oscillating shock waves (Chakrabarti 1990), we need to look for the implications of these shocks as well.

The existence of shocks in the context of accretion flows has been extensively studied after Liang & Thompson (1980) showed that a rotating flow has more than one sonic points just as in a solar wind. Fukue (1987) found an example of a standing shock in Schwarzschild geometry while Nakayama & Fukue (1989) studied transonic flow behaviour in the Kerr geometry without emphasizing on shocks. Chakrabarti (1989) studied the shock properties extensively and classified the parameter space in terms of whether the shock conditions are satisfied or not, both in accretion and in winds. The existence of standing shocks in sub-Keplerian inviscid accretion discs has been tested independently by several groups since then (Nobuta & Hanawa 1994; Yang & Kafatos 1995; Lu & Yuan 1997). The puzzling feature of having two algebraically derived shock locations for a given set of flow parameters was resolved by Nakayama (1992, 1993, 1994, 1995) who showed that one of the shock waves obtained through algebraic study in which the post-shock flow is accelerating must be unstable under infinitesimal perturbation. Time-dependent numerical simulations (which include global and non-linear perturbations) of Chakrabarti & Molteni (1993) in one dimension and Molteni, Lanzafame & Chakrabarti (1994) and

⋆Present address: Indian Institute of Science, Bangalore.
†E-mail: chakraba@bose.res.in

Molteni, Ryu & Chakrabarti (1996b) in two dimensions showed that the so-called unstable shock of Nakayama (1992, 1993, 1994, 1995) does not form at all and the other shock remains stable under axisymmetric perturbations. The theoretical investigation of Chakrabarti (1989) was later fully generalized in the Kerr geometry (Chakrabarti 1996a). Using non-axisymmetric perturbations, Molteni, Toth & Kuznetsov (1999), Okuda et al. (2005), Molteni, Gerardi & Teresi (2006), Gu & Lu (2006), Okuda, Teresi & Molteni (2007) and, more recently, Nagakura & Yamada (2008, 2009) showed that the standing axisymmetric shocks are extremely stable, though non-axisymmetric blobs may anchor them and cause variations in X-ray emissions.

As shown by Chakrabarti (1989, 1996a), for a large region of the parameter space, the standing shocks may form in accretion flows. Chakrabarti (1990) and Chakrabarti (1996b) showed that when the viscosity is increased beyond a critical value the shocks disappear altogether. The existence of a critical viscosity parameter was later verified numerically (Lanzafame et al. 1998). The concept of the viscosity parameter α is also improved (Chakrabarti & Molteni 1995). It is argued that in a generalized flow with a significant radial velocity v, the viscous stress should not be equated to $-\alpha P$ as in SS73, where P is the thermal pressure, but to $-\alpha_\Pi(P + \rho v^2)$ or its vertically integrated value when a disc of vertical equilibrium is considered. Here, ρ is the density and a subscript 'Π' is given to α to distinguish it from the Shakura–Sunyaev viscosity parameter. Using α_Π has the advantage that in a steady flow, the sum of the thermal pressure and ram pressure, i.e. $P + \rho v^2$, is continuous across discontinuities. This makes the viscous stress $w_{r\phi}$ continuous across axisymmetric discontinuities as well.

Subsequently, it has become evident that the standing shocks may be very important in explaining the spectral properties of black hole candidates (Chakrabarti & Titarchuk 1995) as the post-shock region behaves as a boundary layer of a black hole where accreting matter dissipates its thermal energy and generates the hard X-rays by inverse Comptonization. The region is also found to be responsible for the production of relativistic outflows (see Das & Chakrabarti 1999; Das et al. 2001a,b; Fukumura & Kazanas 2007 and references therein). Furthermore, numerical simulations indicated that the shocks may be oscillating in the presence of cooling effects (Molteni, Sponholz & Chakrabarti 1996a) and the shock oscillation solutions appear to explain intricate properties of low- and intermediate-frequency quasi-periodic oscillation (QPOs) (Chakrabarti & Manickam 2000). The power density spectrum (PDS) obtained from several numerical simulations of two-dimensional advective flows (which include cooling processes) also shows the presence of QPOs near the break frequency. The computed PDS is found to be similar to what is observed in black hole candidates (Chakrabarti, Acharyya & Molteni 2004). In some of the stellar mass black holes, e.g. GRO J1655−40 (6.0–6.6 $M_\odot$), XTE 1550−564 (8.4 $M_\odot$), 4U 1630−47 (3 $M_\odot$), high QPO frequencies of 450, 276, 262 Hz, respectively, have been detected. Indeed, the same mechanism of resonance oscillations can be used for all the black holes, from super-massive to stellar mass. The oscillations mentioned here could be radial, vertical or even azimuthal (Molteni et al. 1999, 2006; Okuda et al. 2007; Nagakura & Yamada 2008, 2009). It has also been shown that the shocks oscillate when the Rankine–Hugoniot conditions are not satisfied, especially when the entropy at the inner sonic point is higher than that at the outer sonic point (Ryu, Chakrabarti & Molteni 1997). It is to be noted that the shock oscillations mentioned above are not the signatures of any instability. These are simply time-dependent, stable solutions of the problem very much like an oscillating pendulum.

A sticking point in black hole astrophysics has always been the measurement, or even the estimation, of the spin of the black hole. Chakrabarti (1996b) pointed out that since the location of the shocks is closer in a spinning black hole, the QPO frequency should be higher. Zhang, Cui & Chen (1997), from the observed X-ray properties of the Galactic superluminal jet sources such as GRO J1655−40 and GRS 1915+105, strongly suggest that each of them contains a rapidly spinning black hole. Cui, Zhang & Chen (1998) compared the computed disc precession frequency with that of the observed QPOs and derived the black hole spin for an assumed mass. Applying this model to GRO J1655−40, GRS 1915+105, Cyg X-1 and GS 1124−68, they find that the black holes in GRO J1655−40 and GRS 1915+105 spin at a rate close to the maximum limit, while Cyg X-1 and GS 1124−68 contain only moderately rotating black holes. McClintock (2008) argues that since the radius of the innermost stable circular orbit (ISCO) depends only on the mass and spin of a black hole, the knowledge of the last stable circular orbit could provide a way to estimate the spin, when the mass of the black hole is known, though it is uncertain if a disc ever reaches an ISCO since a boundary condition on the horizon requires that flow must deviate from a Keplerian disc much *before* ISCO (C96b). Such confusion persists as a result, and different groups have given different spin values. In one approach, it is suggested that the disc-dominated state of the black hole binaries has a peak temperature and luminosity that vary together in such a way as to indicate an approximately constant emitting area, and the disc spectral modelling can provide an estimate of the spin of the black hole (Done & Davis 2008; for the spin of the XTE J1550−564, see McClintock 2008). From the fits of the continuum X-ray spectra using the Novikov–Thorne thin disc model of three transient black hole X-ray binaries in the thermal state, it is estimated that dimensionless spin parameter of the black holes would be $a \sim 0.7$–0.85, $a \sim 0.65$–0.8 and $a \sim 0.98$–1 for 4U 1543−47, GRO J1655−40 and GRS 1915+105, respectively (Narayan et al. 2008). These results are different from the fit of multicolour disc blackbody and with the best relativistic model which includes full radiative transfer effects. This approach gives $a \sim 0.1$–0.8 for GRS 1915+105 (Matthew et al. 2006). On the other hand, using inertial-acoustic oscillations Kato & Fukue (2006) found the spins of GRO J1665−40, XTE J1550−564 and GRS 1915+105 to be less than 0.45. Similarly, by fitting the shape of iron line in GX 339−4, Miller et al. (2008) found $a \sim 0.93$. Our approach does not incorporate ISCO and relies on the effects away from it, though we can only provide a range of spin from the observed QPOs.

In the present communication of our series of papers, we wish to study the behaviour of QPOs in a viscous flow around a rotating black hole and discuss how the spins may be estimated. Earlier, Chakrabarti & Das (2004, hereafter CD-2004 and references therein) used pseudo-Newtonian potential $[-1/(x - 2)$, where x is the radial distance from a black hole in units of the Schwarzschild radius] and ignored the rotational effect of the black hole. Here, we use the pseudo-Kerr potential $\Phi_{\rm eff}$ introduced earlier and tested in the previous papers (Chakrabarti & Mondal 2006; Mondal & Chakrabarti 2006; hereafter referred to as Papers I and II, respectively). From the shocks, we directly derive the QPO frequencies as a function of the flow and the black hole parameters. In the next section, we present the governing equations of the flow. Unlike the case of an inviscid flow where the specific energy and the angular momentum remain the same at the sonic points, in our present case, both of them vary and the analysis is more complex. In Section 3, we present the sonic point analysis and in Section 4, we present the method of computing the shock locations and from that the QPO

frequencies. Finally, in Section 5, we discuss the implications of our results and draw concluding remarks.

2 GOVERNING EQUATIONS OF THE FLOW

We describe a viscous, axisymmetric accretion flow around a rotating black hole by an effective potential $\Phi_{\rm eff}$ (PK potential). We consider the units of velocity, distance and time to be c, $r_g = GM_{\rm BH}/c^2$ and $GM_{\rm BH}/c^3$, respectively, where c is the velocity of light, and G and $M_{\rm BH}$ are the gravitational constant and mass of the black hole, respectively. In this unit, distances are $x = r/r_g$. In our model of the disc which is assumed to be in hydrostatic equilibrium in the vertical direction (VEM), local disc height is obtained by equating the pressure gradient force in the VEM with the component of the gravitational force in that direction. The height H_0 of the disc is obtained as

$$H_0(x) = \frac{a_{\rm s} x^{\frac{1}{2}}}{\gamma}\left[\frac{\partial \Phi_{\rm eff}(x,z)}{\partial z}\right]^{-\frac{1}{2}}_{z=0}. \tag{2.1}$$

Here, $a_{\rm s}$ is the adiabatic sound speed defined as $a_{\rm s} = \sqrt{\gamma P/\rho}$. We assume that in the VEM, the angular momentum changes very little. As discussed in the Introduction, we shall use the viscosity prescription of Chakrabarti & Molteni (1995) valid for flows with significant radial motion. Thus, the viscous stress is

$$W_{x\phi} = -\alpha_\Pi \Pi \text{ and } \Pi = [W + \Sigma v^2]. \tag{2.2}$$

Here, W and Σ are the vertically integrated pressure and density of the flow. As mentioned before, this will ensure that the viscous stress is continuous across the axisymmetric shock wave that we are studying here.

In the steady state, the dimensionless hydrodynamic equations that govern the infalling matter are the followings (C96b and CD2004).

(a) The continuity equation is obtained from the mass flux of the flow $\dot{M} = \Sigma x v$ and is given by

$$\frac{\rm d}{{\rm d}x}[\Sigma x v] = 0. \tag{2.3a}$$

$$\frac{1}{v}\frac{{\rm d}v}{{\rm d}x} + \frac{1}{a_{\rm s}}\frac{{\rm d}a_{\rm s}}{{\rm d}x} + \frac{\rm d}{{\rm d}x}\log\rho = -\frac{H'}{H}, \tag{2.3b}$$

where $H(x) = h(x)x$ and $h(x)$ is calculated from the relation $H_0 = a_{\rm s}h(x)$, where H_0 is the vertical height of the disc.

(b) The Euler equation in terms of the $a_{\rm s}(= \sqrt{\gamma P/\rho})$ yields

$$v\frac{{\rm d}v}{{\rm d}x} + \frac{2a_{\rm s}}{\gamma}\frac{{\rm d}a_{\rm s}}{{\rm d}x} + \frac{a_{\rm s}^2}{\gamma}\frac{\rm d}{{\rm d}x}\log\rho = -\frac{\rm d}{{\rm d}x}\Phi_{\rm eff}, \tag{2.4}$$

where $\Phi_{\rm eff}$ is our usual effective PK potential (Papers I and II).

(c) The entropy generation equation is

$$\Sigma v T\frac{{\rm d}s}{{\rm d}x} = Q^+ - Q^-. \tag{2.5}$$

In the present analysis, we ignore cooling effects explicitly, i.e. $Q^- = 0$ is used. Assuming an equation of state valid for an ideal gas, equation (2.5) takes the form

$$\frac{I_n v a_{\rm s}^2}{\gamma}\left[\frac{2n}{a_{\rm s}}\frac{{\rm d}a_{\rm s}}{{\rm d}x} - \frac{1}{\rho}\frac{{\rm d}\rho}{{\rm d}x}\right] = \frac{-Q^+}{\rho h} = -H. \tag{2.6}$$

We calculate H using the MISStress prescription for Q^+ according to which

$$Q^+ = \frac{W_{x\phi}^2}{\eta} = \frac{W_{x\phi}^{(1)}W_{x\phi}^{(2)}}{\eta} = (-\alpha_\Pi\Pi)\left(x\frac{{\rm d}\Omega}{{\rm d}x}\right).$$

In this case, H takes the form

$$H = A\left(ga_{\rm s}^2 + \gamma v^2\right)\left(x\frac{{\rm d}\Omega}{{\rm d}x}\right) = A\Theta\left(x\frac{{\rm d}\Omega}{{\rm d}x}\right), \tag{2.7}$$

where $g = \frac{I_{n+1}}{I_n} = \frac{2\gamma}{(3\gamma-1)}$, $\Theta = (ga_{\rm s}^2 + \gamma v^2)$ and $A = -\frac{\alpha_\Pi}{\gamma}$. Here, $\Omega(x)$ is the angular velocity of the accreting matter at the radial distance x and $n(= \frac{1}{\gamma-1})$ is the polytropic index. I_n and I_{n+1} come from the definition of the vertically averaged density and pressure (Matsumoto et al. 1984).

(d) The azimuthal momentum equation is

$$\frac{{\rm d}l}{{\rm d}x} = -\frac{1}{\Sigma x v}\frac{\rm d}{{\rm d}x}\left(x^2 W_{x\phi}\right) = -\frac{\rm d}{{\rm d}x}\left(\frac{x W_{x\phi}}{\Sigma v}\right). \tag{2.8a}$$

Putting $W_{x\phi} = -\alpha_\Pi\Pi$ and $\Pi = [W + \Sigma v^2]$, the integration of the above equation yields

$$l = l_{\rm in} + \frac{\alpha_\Pi x}{\gamma v}\left(ga_{\rm s}^2 + \gamma v^2\right). \tag{2.8b}$$

$l = l_{\rm in}$ at the inner edge of the disc ($x = 0$). Here, we use the constant mass flux as $\sim\Sigma\, x v$. It is evident that $\alpha_\Pi = 0$ implies $l = l_{\rm in}$ which is a conserved quantity for an inviscid flow.

In a general relativistic flow around a black hole, it is not $-u_\phi$, but the ratio $-u_\phi/u_t$ conserved, where u_μ are the velocity components. The specific angular momentum $\tilde{l}$ that is used in our PK potential is supposed to be conserved for the particle dynamics only (similar to '$-u_\phi$' in a general relativistic flow). However, for a flow, we need to divide by the specific binding energy. Also as seen from a large distance, the flow would be dragged with an angular momentum ωx^2 which remains non-zero even when the matter angular momentum is zero. Hence, for flow dynamics, we use

$$l = \left.\frac{(\tilde{l} + \omega x^2)}{\Phi_{\rm eff}}\right|_{\rm PK} = \left.\left(l + \frac{\omega x^2}{\Phi_{\rm eff}}\right)\right|_{\rm PK}$$
$$= (l + s)|_{\rm PK} = j|_{\rm PK},$$

where $s = \frac{\omega x^2}{\Phi_{\rm eff}}$ and $j = (1 + s) = \Omega x^2$ is an 'effective angular momentum' due to the dragging effect of the Kerr black hole.

Finally, the differential form of equation (2.8a) is given by

$$\frac{1}{x}\frac{{\rm d}j}{{\rm d}x} = \alpha_\Pi\left(1 - \frac{ga_{\rm s}^2}{\gamma v^2}\right)\frac{{\rm d}v}{{\rm d}x} + \frac{2\alpha_\Pi g a_{\rm s}}{\gamma v}\frac{{\rm d}a_{\rm s}}{{\rm d}x} + \frac{\alpha_\Pi}{\gamma v x}\left(ga_{\rm s}^2 + \gamma v^2\right). \tag{2.9}$$

3 ANALYSIS OF THE SONIC POINT CONDITIONS

Since the outer edge of the accretion disc occurs at a very large distance, the matter starts with an almost zero radial velocity even though it enters into the black hole with the velocity of light c. Thus, during accretion, at some point, matter velocity should exactly match with the sound speed. This point is called a critical point or a sonic point. When matter crosses a sonic point, it becomes transonic. For the sake of completeness, we carry out the sonic point analysis by representing above three equations, namely equations (2.3), (2.4)

and (2.5), in the matrix form given by

$$\begin{pmatrix} A\alpha_\Pi \dfrac{(\gamma^2 v^4 - g^2 a_s^4)}{v^3 a_s^2} & \left[\dfrac{2}{(\gamma-1)a_s} + \dfrac{2A\alpha_\Pi g}{a_s v^2}\Theta\right] & -1 \\ \dfrac{1}{v} & \dfrac{1}{a_s} & 1 \\ v & \dfrac{2a_s}{\gamma} & \dfrac{a_s^2}{\gamma} \end{pmatrix}$$

$$\begin{pmatrix} \dfrac{\mathrm{d}v}{\mathrm{d}x} \\ \dfrac{\mathrm{d}a_s}{\mathrm{d}x} \\ \dfrac{\mathrm{d}}{\mathrm{d}x}\log\rho \end{pmatrix} = \begin{pmatrix} -A\Theta\left[\dfrac{\alpha_\Pi}{v^2 a_s^2 x}\Theta - \dfrac{2\gamma j}{v a_s^2 x^2}\right] \\ -\dfrac{H'}{H} \\ -\Phi'_{\rm eff} \end{pmatrix}. \tag{3.1}$$

The determinant (D) of the square matrix is

$$D = -\frac{1}{a_s v^2}\left[\frac{2a_s^2 v}{(\gamma-1)} - \left(\frac{\gamma+1}{\gamma-1}\right)v^3 - A\alpha_\Pi v\Theta\left\{(2g-1) - \frac{g a_s^2}{\gamma v^2}\right\}\right]. \tag{3.2}$$

The numerator (N) of $\frac{\mathrm{d}v}{\mathrm{d}x} = \frac{N}{D}$ can be calculated from the square matrix

$$\begin{pmatrix} -A\Theta\left[\dfrac{\alpha_\Pi}{v^2 a_s^2 x}\Theta - \dfrac{2\gamma j}{v a_s^2 x^2}\right] & \left[\dfrac{2}{(\gamma-1)a_s} + \dfrac{2A\alpha_\Pi g}{a_s v^2}\Theta\right] & -1 \\ -\dfrac{H'}{H} & \dfrac{1}{a_s} & 1 \\ -\Phi'_{\rm eff} & \dfrac{2a_s}{\gamma} & \dfrac{a_s^2}{\gamma} \end{pmatrix}. \tag{3.3}$$

The numerator (N) is the determinant of the square matrix. Some simplification yields

$$N = -\frac{1}{a v^2}\left[-\frac{A\alpha_\Pi}{\gamma x}\Theta^2 + \frac{2Ajv}{x^2}\Theta + \Phi'_{\rm eff}\left(\left(\frac{\gamma+1}{\gamma-1}\right)v^2 + 2A\alpha_\Pi g\Theta\right) - \frac{2v^2 a_s^2}{(\gamma-1)}\frac{H'}{H} - \frac{2A\alpha_\Pi g a_s^2}{\gamma}\Theta\frac{H'}{H}\right]. \tag{3.4}$$

Note that in case of pseudo-Newtonian potential, we have

$$\Phi'_{\rm eff} = -\left(\frac{l^2}{x^3} - \frac{1}{2(x-1)^2}\right) \quad \text{and} \quad H = x^{\frac{3}{2}}(x-1),$$

$$\text{i.e.} \quad \frac{H'}{H} = \frac{3}{2x} + \frac{1}{(x-1)} = \frac{(5x-3)}{2x(x-1)},$$

and therefore by inserting the above values in the numerator (N) the form of $\frac{\mathrm{d}v}{\mathrm{d}x} = \frac{N}{D}$ becomes identical as obtained in CD2004.

At the sonic points, both the numerator and the denominator must vanish simultaneously. For $D = 0$, one can get the expression for the Mach number $M(x_c) = v/a_s$ at the sonic point and is given by

$$M^2(x_c) = \frac{-m_b - \sqrt{m_b^2 - 4m_a m_c}}{2m_a} \tag{3.5a}$$

where

$$m_a = -A\alpha_\Pi\gamma^2(\gamma-1)(2g-1) - \gamma(\gamma+1), \tag{3.5b}$$

$$m_b = -2\gamma - 2A\alpha_\Pi g\gamma(\gamma-1)(g-1), \tag{3.5c}$$

$$m_c = A\alpha_\Pi g^2(\gamma-1). \tag{3.5d}$$

In the weak viscosity limit, $\alpha_\Pi \to 0$ and the Mach number at the sonic point $M(x_c) \approx \sqrt{\frac{2n}{2n+1}}$ which is our usual result. Setting $N = 0$ at the sonic point, we get a polynomial for the sound speed as the angular momentum is also a function of the sound speed a_s and the velocity v which appears in the numerator (N). Depending on the initial parameters, namely the specific energy and the specific angular momentum at the inner edge, a flow may have multiple sonic points. Nature of sonic point depends on the velocity gradients at the sonic point. Variation of energy $\mathcal{E}$ and angular momentum with the flow at the sonic point distance (X_c) is shown in Figs 1(a)–(b). The viscosity parameter α_Π and the Kerr parameter (a) are assumed to be 0.05 and 0.50, respectively. The curves in Fig. 1(a) are drawn for the different values of angular momentum at the inner edge ($l_{\rm in}$). These are $l_{\rm in} = 2.3$, 2.4, 2.5, 2.6, 2.7, 2.8, 2.9, 3.0 and 3.1 (from top to bottom). At a very large distance, all the curves asymptotically merge to unity which is the rest-mass energy of the flow. For a very low angular momentum at inner edge, the flow may have one sonic point solution whereas at a very high low angular momentum, the flow may have one or two sonic points depending on the energy of the flow. For moderate values of the angular momentum at the inner edge, a flow may have transonic solution which was the common feature in the inviscid flow. The minimum and maximum values of the curves correspond to the extreme locations of the inner (I) and the outer (O) sonic point. In between, the flow may have another spiral type middle (M_d) sonic point (Abramowicz & Kato 1989). Stable, unstable or oscillating shock may form in between the middle (M_d) and the outer (O) sonic points as well as in between

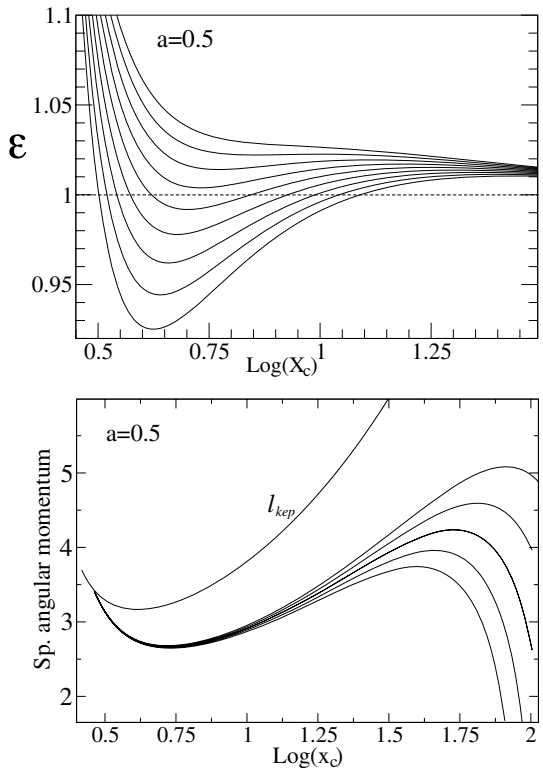

Figure 1(a–b) Variation of (a) specific energy and (b) specific angular momentum of the flow at the sonic point distance (X_c). Curves in (a) are drawn for the different values of angular momentum at the inner edge which is constant. These are considered as $l_{\rm in} = 2.3, 2.4, 2.5, 2.6, 2.7, 2.8, 2.9, 3.0$ and 3.1 (from top to bottom). Curves in (b) are for the energy values $\mathcal{E}_i = 1.004$, 1.005, 1.006, 1.007 and 1.008 (from top to bottom). The viscosity parameter is $\alpha_\Pi = 0.05$.

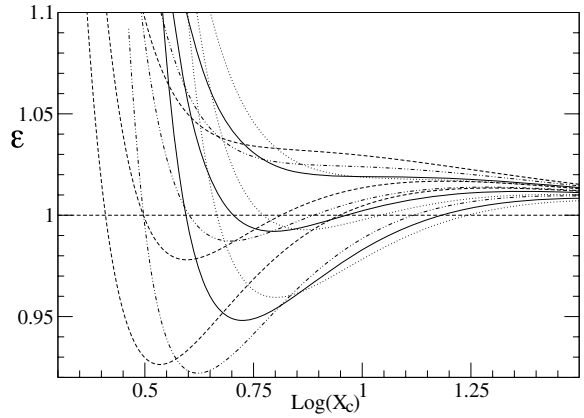

Figure 2. A comparison of the variation of the specific energy of the flow at the sonic point X_c when the spin parameter is changed. The spin parameter a and the $l_{\rm in}$ (from top to bottom) used are 0, (2.6, 3.1, 3.5) (dotted), $a =$ 0.25, (2.5, 2.9, 3.3) (solid), 0.5, (2.3, 2.7, 3.1) (dash–dotted) and $a = 0.75$, (2.1, 2.3, 2.7) (dashed), respectively. The viscosity parameter is $\alpha_\Pi = 0.05$. Note that the range of angular momentum of interest shifts with the spin parameter.

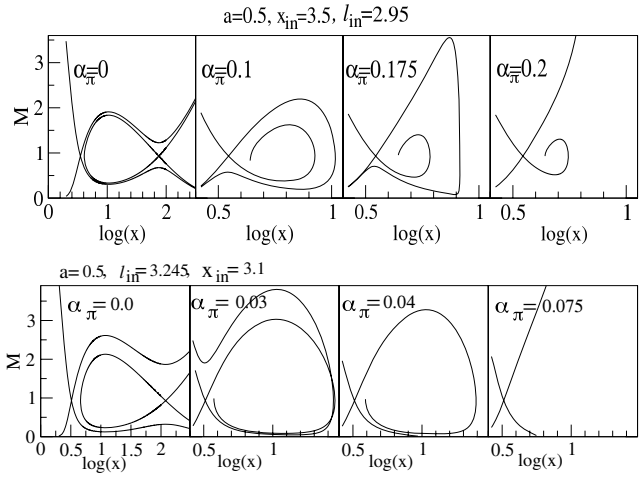

Figure 3. (a–b) Variation of the global solution topologies with the viscosity parameter α_Π of (a) wind to accretion and (b) wind is shown for a moderate value of the Kerr parameter ($a = 0.5$). The other required parameters are the same as those used in Figs 1(a)–(b).

the inner (I) sonic point and the middle (M_d) sonic points, respectively. The locations of the middle (M_d) sonic point corresponds to the extreme shock locations. The issue of shock formation will be discussed later in details. Kato, Honma & Matsumoto (1988a,b) discussed pulsational instabilities in shock-free flows. Numerical simulation of two-dimensional magnetohydrodynamic flows shows such instabilities and these have been used to explain QPOs (Kato 2004) in certain objects.

In Fig. 1(b), we show the plots of specific angular momentum versus sonic point locations (X_c). Different curves are drawn for the energy values $\mathcal{E}_i = 1.004$, 1.005, 1.006, 1.007 and 1.008 (from top to bottom). The viscosity and Kerr parameters are identical to those for Fig. 1(a).

In order to show the variation of the critical energies required to pass through the sonic points, we show in Fig. 2 plots of $\mathcal{E}$ versus (X_c) for various specific angular momentum when the spin parameters are varied. The spin a and the $l_{\rm in}$ (from top to bottom) used for the plots are 0, (2.6, 3.1, 3.5) (dotted), 0.25, (2.5, 2.9, 3.3) (solid), 0.5, (2.3, 2.7, 3.1) (dash–dotted) and 0.75, (2.1, 2.3, 2.7) (dashed), respectively. The viscosity parameter is $\alpha_\Pi = 0.05$. Note that the range of angular momentum of interest shifts with the spin parameter. We did not plot for higher spin values since our pseudo-potential is not accurate for $a > 0.8$ (see Paper I).

For a given set of flow parameters comprising the angular momentum at the inner edge, the energy or the sonic point locations together with viscosity (α_Π) and the Kerr parameter (a), one can numerically solve equation (3.1) to get different solution topologies. We have presented here variation of such topologies with the viscosity parameter keeping other flow parameters fixed. We call the solutions 'accretion-like' when the corresponding inviscid solution passes through the outer sonic point and 'wind-like' when the corresponding inviscid solution passes through the inner sonic point. Figs 3(a)–(b) show the variation of solution topologies with the viscosity parameter (α_Π) of (a) the wind converted to accretion ($\alpha_\Pi =$ 0.0, 0.1, 0.175, 0.2) and (b) wind ($\alpha_\Pi = 0.0, 0.03, 0.04, 0.075$) for a moderate value of the Kerr parameter ($a = 0.5$). The other required parameters are $X_{\rm in} = 3.5$, $l_{\rm in} = 2.95$ for accretion and $X_{\rm in} = 3.1$, $l_{\rm in} = 3.245$ for wind. Figs 3(a)–(b) also indicate that there exists a critical value of the viscosity parameter beyond which no physical solutions of topologies are possible in accretion or wind flows.

4 METHOD OF CALCULATING THE SHOCK LOCATIONS

During the integration along the subsonic branch, it is possible to calculate all the local variables (i.e. v, $a_{\rm s}$, M, ρ) at the post-shock region, in terms of the initial flow parameters. We calculate the local pressure, local specific energy and specific angular momentum at the shocks using these subsonic local variables. At the shock, the total pressure (thermal plus ram), the flow energy, the mass accretion rate and the specific angular momentum are conserved. These conserved quantities at the shock give the other set of local variables for the supersonic branch.

This set of local variables on the supersonic branch help us to get outer sonic point uniquely for an accretion flow when the inner sonic point and other initial flow parameters are supplied. Thus, the accretion flow can be connected with both the saddle type sonic points through a shock for a dissipative system, and this determines the standing shock location for a given set of initial parameters.

We compute the local flow variables on the supersonic branch in terms of the subsonic local flow variables in the following way.

Our model accretion flow is in vertical equilibrium and the total pressure of the accretion flow at any given point is given by

$$\Pi = W + \Sigma v^2.$$

The above equation combined with the continuity equation gives

$$a_{\rm s}^2 = \frac{\gamma x \Pi}{\dot{M} g} v - \frac{\gamma}{g} v^2 = \kappa_1 \kappa_2 v - \kappa_2 v^2, \tag{4.1}$$

where $\kappa_1 = \frac{x\Pi}{\dot{M}}$ and $\kappa_2 = \frac{\gamma}{g}$. From the local flow energy equation, radial velocity v at shock location in the supersonic branch can be calculated using the expression for $a_{\rm s}$ and is given by

$$v = \frac{-v_b + \sqrt{v_b^2 - 4 v_a v_c}}{2 v_a}, \tag{4.2}$$

where $v_a = 2n\kappa_2 - 1$, $v_b = -2n\kappa_1\kappa_2$ and $v_c = 2(\mathcal{E} - \Phi_{\rm eff})$. Here, total pressure and flow energy at the shock location are calculated with the help of the subsonic flow variables. We consider only the

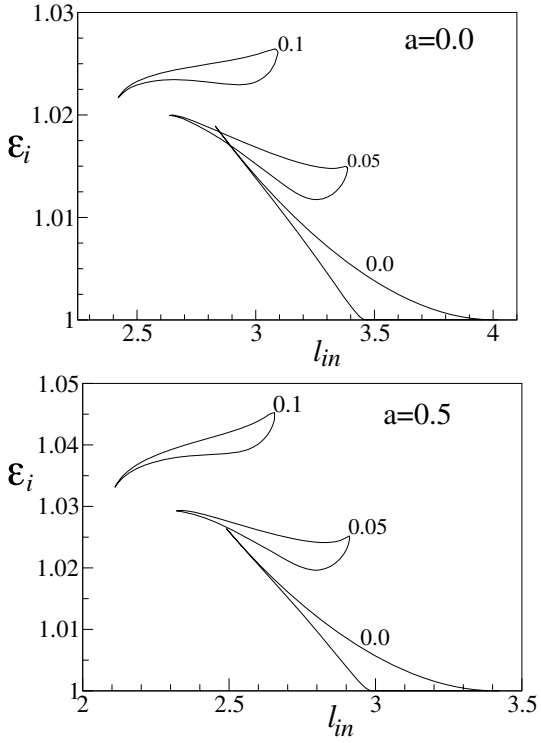

Figure 4. (a–b) Variation of the parameter space spanned by the energy (at inner sonic point) and angular momentum (at the inner edge) for the different viscosity parameter $\alpha_\Pi = 0.0$, 0.05, 0.1. The values of the Kerr parameter are (a) $a = 0.0$ and (b) $a = 0.5$.

'+' sign as we are interested in getting the local flow variables in the supersonic branch. This radial velocity is used to get the sound speed a_s in the supersonic branch of the flow. We use supersonic flow variables (v and a_s) to get the outer sonic point by numerical integration, and it completes the accretion flow solution having a shock. The collection of flow parameters which yield solutions with shocks belongs to a continuous region of parameter space spanned by the energy $\mathcal{E}_i$ (inner sonic point) and angular momentum $l_{\rm in}$. The investigation of these parameter space ($\mathcal{E}_i - l_{\rm in}$) is made for both the Schwarzschild (the Kerr parameter $a = 0.0$) and the Kerr spacetime (for a moderate value of the Kerr parameter $a = 0.5$) and are shown in Figs 4(a)–(b). Similar investigation of parameter space is also made for different viscosity parameter ($\alpha_\Pi = 0.0, 0.05, 0.1$). We observe that the basic features are almost similar; however the black hole rotation has noticeable effects on the shape and location of the regions of parameter space ($\mathcal{E}_i - l_{\rm in}$) in which the accretion shock may form. The different regions of the parameter space shrink as the viscosity parameter α_Π increases. The region also moves up to the higher energy region. In Fig. 5, we show how the parameter space varies with spin when the viscosity parameter is kept fixed at $\alpha_\Pi = 0.05$. With the increase in the Kerr parameter, the region shifts towards higher energy and lower angular momentum. However, the overall shape remains almost unchanged. Fig. 6 shows an example of a solution topology of an accretion flow containing a shock at $X_s = 21.44$. The other flow parameters are $\alpha_\Pi = 0.05, l_{\rm in} = 2.8$, $X_i = 3.5235, a = 0.5$. The derived outer sonic point is at $X_{\rm out} = 355.10$. For a sufficiently high viscosity, the Rankine–Hugoniot conditions for the steady shock is no longer satisfied anywhere in the flow and the parameter space of interest disappears.

Numerical simulations indicate that the shocks may be oscillating when the regions close to the steady shock formation region are considered, especially when there are two saddle-type sonic points (with the entropy at the inner sonic point higher than that at the outer sonic point) but the Rankine–Hugoniot conditions are not satisfied anywhere between those two sonic points (Ryu, Chakrabarti & Molteni 1997). In the presence of cooling effects (Molteni et al. 1996a), the shocks also exhibit oscillations. As mentioned in the Introduction, non-axisymmetric oscillations are also possible. These time-dependent solutions may be very important in explaining QPOs for all the black holes, from stellar mass to super-massive.

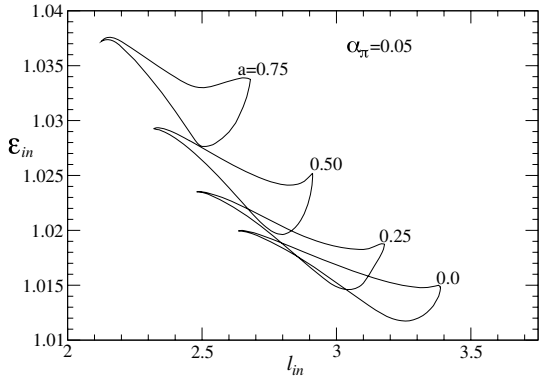

Figure 5. Variation of the parameter space spanned by the energy (at inner sonic point) and angular momentum (at the inner edge) for the different spin parameter (marked) when viscosity parameter is kept constant $\alpha_\Pi = 0.05$. As the spin is increased, one requires higher energy but lower angular momentum to have shocks in the flow.

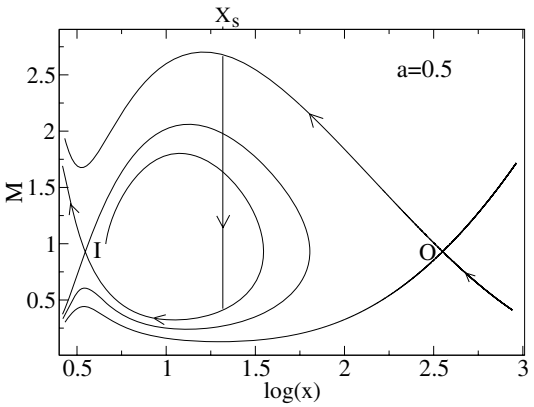

Figure 6. An example of the solution topology which contains a shock at $X_s = 21.44$. The flow parameters are $\alpha_\Pi = 0.05, l_{\rm in} = 2.8, X_{\rm in} = 3.5235$ and $a = 0.5$. The location of the derived outer sonic point $X_{\rm out}$ is 355.10.

We observe that the post-shock variables depend on the flow parameters in an accretion flow topology. The topology obtained from the physical parameters of the flow variable helps us to determine the shock locations and the post-shock variables such as post-shock velocity, Mach no. and so on. The post-shock velocity profile after the shock helps us to determine the infall time of matter falling to the black hole using

$$t_{\rm infall} = \int {\rm d}t = \int \frac{{\rm d}x}{v},$$

where $v = v(x)$ is obtained from the flow solution. The final point of integration is taken to be the inner sonic point as the time taken from the sonic point to the horizon is negligible.

Since in a resonance oscillation model (Molteni et al. 1996a; Chakrabarti et al. 2004) the oscillation period T is the infall time,

the frequency of QPO is given by

$$\nu_{\rm QPO} = \frac{1}{T_{\rm QPO}} = \frac{1}{t_{\rm infall}}.$$

Here, time is given in the geometrical unit. To estimate the QPO frequency in hertz, we convert the infall time $t_{\rm infall}$ to have a dimension of seconds by multiplying with r_g/c. For the sake of concreteness, we use the mass of the black hole to be $10\,{\rm M}_\odot$. For an arbitrary mass black hole $M_{\rm BH}$, this is to be multiplied by $m_{10} = \frac{M_{\rm BH}}{10\,{\rm M}_\odot}$.

Figs 7(a)–(b) show variations of the angular momentum ($l_{\rm in}$) at the inner edge with (a) the extreme shock locations ($X_{\rm s}$) and (b) the extreme QPO frequency for a $10\,{\rm M}_\odot$ black hole. What this means is that each point on a curve is drawn for that specific energy which will produce a shock which is as close to the black hole as possible. Parameter pairs of (a, α_Π) are marked on various curves. In Fig. 7(a), we note that the extreme shocks occur almost at the same locations when we compare the viscous and non-viscous accretion flows for fixed Kerr parameter values (here $a = 0.0$ or 0.50). In fact, it is closer for inviscid flow. In Fig. 7(b), the oscillation frequencies of the shocks located at extreme points are calculated from the infall time. Most interestingly, the QPO frequency has larger values for the viscous flows although the shock locations ($X_{\rm s}$) are closer for inviscid flows (Fig. 7a). The angular momentum at the shock shifts to a lower value as one increases viscosity. As a result, the post-shock velocity increases with the increase of the viscosity parameter.

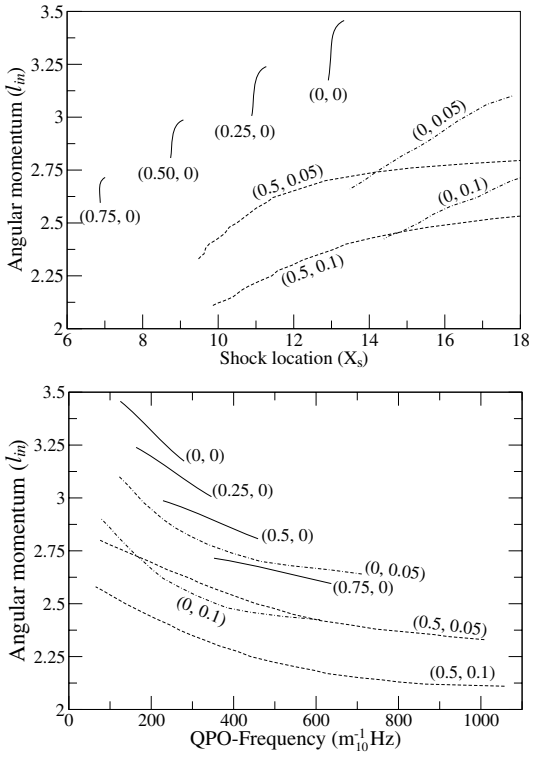

Figure 7. (a–b) Variation of the angular momentum ($l_{\rm in}$) with (a) the extreme (closest to the black hole) shock locations ($X_{\rm s}$) and (b) the extreme (highest) QPO frequency for a $10\,{\rm M}_\odot$ black hole. Parameter pairs (a, α_Π) are marked on various curves. In (b), the oscillation frequency of the extreme shock location (which is the QPO frequency in the present model) is provided. Comparing the viscous and non-viscous accretion flows for $a = 0.0$ or 0.50, it is observed that the extreme shocks occur almost at the same locations independent of viscosity parameter, though for higher a, the extreme shock location is closer and thus the highest QPO frequency is higher. Here $m_{10} = \frac{M_{\rm BH}}{10\,{\rm M}_\odot}$.

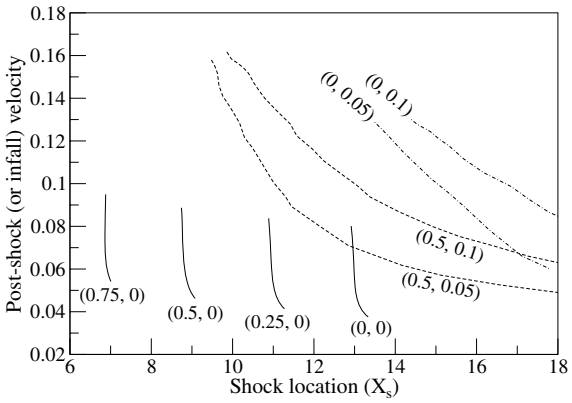

Figure 8. Plots of the post-shock velocity of infalling matter versus shock locations for various pair of parameters (a, α_Π). The post-shock velocity or the infall velocity at the shock is much higher in case of high viscous flow and high spin of the black hole. Higher infall velocity implies a shorter infall time and thus a QPO of higher frequency.

Also note that QPOs have higher values when the parameter pairs (a, α_Π) are (0, 0.05) and (0.5, 0.1). This imply that depending on the spin parameter there exists certain critical values of viscosity parameter (α_Π) for which the oscillation frequency is maximum. This parameter is solely governed by the spin of the black hole.

In Fig. 8, we show the post-shock velocity of the flow as a function of the shock location. What we observe is that for extreme QPO frequencies, the shock location should be the lowest, as expected. However, after the initial changes at lower viscosity, the sensitivity on the higher values of the viscosity parameter to the extreme frequency is not very much. We marked (a, α_Π) on each curve as before. The velocity at the post-shock flow is higher for higher viscosities, and thus the infall time also becomes shorter and the corresponding QPO frequency becomes higher. In passing, we may note that in an inviscid flow, though the shock location changes very much, the velocity at the shock location does not change by the same proportion.

5 DISCUSSIONS AND CONCLUSIONS

The results obtained by our analysis show that the general features of accretion flow observed in Schwarzschild space-time remain almost similar for accretion flows in the Kerr space-time too. However, the black hole rotation has some noticeable effects on the shape and location of the regions of parameter space (energy versus angular momentum) where shocks in accretion may form. We observe that as the Kerr parameter increases the parameter spaces obtained for feasible variation of the viscosity parameter shifts towards the region of higher energy and lower angular momentum while their shape remains almost unchanged.

We found that as the viscous dissipation reduces the angular momentum of the infalling matter, the post-shock velocity becomes higher and thus infall time becomes shorter, which in turn produces high-frequency QPOs. Thus, the viscosity allows the possibility to have higher QPO frequency. Similarly, the spin of black hole also enhances QPO frequency and depending on the spin of black hole, there exists a critical viscosity for which QPO frequency is extremum. In this work, we ignored the cooling effects which tend to reduce the shock location, and thus the QPO frequencies should increase. This will be studied elsewhere.

What is the implication of our work in constraining, if at all, the spin of a black hole? From Fig. 7(b), we observe that low-frequency QPOs can always be fitted with black holes of both high and low spins, simply because what we are plotting are the *highest possible* QPO frequencies. However, a lower limit of a could be obtained from the highest QPO observed from a system. For instance, Fig. 7(b) clearly shows that an observed frequency of, say, 300, 400, 500, 700 Hz would imply a to be larger than 0, 0.25, 0.5 and 0.75, respectively, if the viscosity is low enough. Numerical simulations to compute viscosity parameter has also shown that α_{Π} is usually 0.01 or less. Thus, our lower limit of a is very robust and at least it proves that the black hole is definitely *spinning*! Furthermore, the pseudo-Kerr potential is more credible for lower a values anyway (see Papers I and II), and thus such conclusions are probably correct as far as the lower limits go. Comparing shock locations in full general relativity and in the pseudo-Kerr treatment, we already showed that they agree within a few per cent. An error of 5 per cent in the shock location will produce an error of 7.5 per cent in QPO frequency, and thus a similar error in the Kerr parameter. The future goal should therefore be to obtain the highest possible QPO frequency from a given object and put a lower limit on the spin parameter.

ACKNOWLEDGMENTS

PB is supported by a CSIR fellowship and SKC is partly supported by a RESPOND project.

REFERENCES

Abramowicz M. A., Kato S., 1989, ApJ, 336, 304
Chakrabarti S. K., 1989, ApJ, 347, 365
Chakrabarti S. K., 1990, Theory of Transonic Astrophysical Flows. World Scientific, Singapore
Chakrabarti S. K., 1996a, ApJ, 472, 237
Chakrabarti S. K., 1996b, ApJ, 464, 664 (C96b)
Chakrabarti S. K., Das S., 2004, MNRAS, 349, 649 (CD-2004)
Chakrabarti S. K., Manickam S. G., 2000, ApJ, 531, L41
Chakrabarti S. K., Molteni D., 1993, ApJ, 417
Chakrabarti S. K., Molteni D., 1995, MNRAS, 272, 80
Chakrabarti S. K., Mondal S., 2006, MNRAS, 369, 976 (Paper I)
Chakrabarti S. K., Titarchuk L. G., 1995, ApJ, 455, 623 (CT95)
Chakrabarti S. K., Acharyya K., Molteni D., 2004, A&A, 421, 1
Cui W., Zhang S. N., Chen W., 1998, ApJ, 492, L53
Das T. K., Chakrabarti S. K., 1999, Class. Quant. Grav., 16, 3879
Das S., Chattopadhyay I., Nandi A., Chakrabarti S. K., 2001, A&A, 379, 683
Done C., Davis S. W., 2008, ApJ, 683, 389
Fukue J., 1987, PASJ, 39, 309
Fukumura K., Kazanas D., 2007, ApJ, 669, 1
Gu W.-M., Lu J.-F., 2006, MNRAS, 365, 647
Kato Y., 2004, PASJ, 56, 931
Kato S., Fukue J., 2006, PASJ, 58, 909
Kato S., Honma F., Matsumoto R., 1988a, MNRAS, 231, 37
Kato S., Honma F., Matsumoto R., 1988b, PASJ, 40, 709
Lanzafame G., Molteni D., Chakrabarti S. K., 1998, MNRAS, 299, 799
Liang E. P. T., Thompson K. A., 1980, ApJ, 240, 271
Lu J. F., Yuan F., 1997, PASJ, 49, L525
McClintock J. E., 2008, 10th Meeting of the High Energy Astrophysics Division (HEAD) of the American Astronomic Society, 31 March–2 April 2008, Los Angeles, CA, 14.01
Matsumoto R., Kato S., Fukue J., Okazaki A. T., 1984, PASJ, 36, 7
Middleton M., Done C., Gierlinski M., Davis S. W., 2006, MNRAS, 373, 1004
Miller J. M. et al., 2008, ApJ, 679, L113
Molteni D., Lanzafame G., Chakrabarti S. K., 1994, ApJ, 425, 161
Molteni D., Sponholz H., Chakrabarti S. K., 1996a, ApJ, 457, 805
Molteni D., Ryu D., Chakrabarti S. K., 1996b, ApJ, 470, 460
Molteni D., Toth G., Kuznetsov A., 1999, ApJ, 516, 411
Molteni D., Gerardi G., Teresi V., 2006, MNRAS, 365, 1405
Mondal S., Chakrabarti S. K., 2006, MNRAS, 371, 1418 (Paper II)
Nagakura H., Yamada S., 2008, ApJ, 689, 391
Nagakura H., Yamada S., 2009, ApJ, in press
Nakayama K., 1992, MNRAS, 259, 259
Nakayama K., 1993, PASJ, 45, 167
Nakayama K., 1994, MNRAS, 270, 871
Nakayama K., 1996, MNRAS, 281, 226
Nakayama K., Fukue J., 1989, PASJ, 41, 271
Narayan R., M$^{\rm c}$Clintock J. E., Shafee R., 2008, in Yuan Y.-F., Li X.-D., Lai D., eds, AIP Conf. Proc. Vol. 968, Astrophysics of Compact Objects. AIP, New York, p. 265
Nobuta K., Hanawa T., 1994, PASJ, 46, 257
Okuda T., Teresi V., Toscano E., Molteni D., 2005, in Bulik N. T., Rudak N. B., Madejski G., eds, AIP Conf. Proc. Vol. 801, Astrophysical Sources of High Energy Particles and Radiation. Am. Inst. Phys., New York, p. 395
Okuda T., Teresi V., Molteni D., 2007, MNRAS, 377, 1431
Paczynski B., Wiita P. J., 1980, A&A, 88, 23
Ryu D., Chakrabarti S. K., Molteni D., 1997, ApJ, 474, 378
Shakura N. I., Sunyaev R. A., 1973, A&A, 24, 337 (SS73)
Smith D. M., Heindl W. A., Marwardt C. B., Swank J. H., 2001, ApJ, 554, L41
Smith D. M., Heindl W. A., Swank J. H., 2002, ApJ, 569, 362
Wu K., Soria R., 2002, ApJ, 565, 1161
Yang R., Kafatos M., 1995, A&A, 295, 238
Zhang S. N., Cui W., Chen W., 1997, ApJ, 482, L155

This paper has been typeset from a TEX/LATEX file prepared by the author.